IFPRI
PAPUA NEW GUINEA

WORKING PAPER JANUARY 2026

Creating a Taro Yield Emulator and Using it to Study Climate Change Impact on Taro in Papua New Guinea

Tamunotonye M. Braide, Timothy S. Thomas, and Richard D. Robertson

CONTENTS

TABLES

FIGURES

ABSTRACT

This paper develops a taro yield emulator to assess climate change impacts on taro production in Papua New Guinea (PNG). The emulator uses a fixed-effects polynomial regression trained on DSSAT simulations to capture non-linear, stage-specific responses of taro yields to rainfall and temperature. Historical MSWX weather and future climates from CMIP6/ISIMIP3b and a large MIT-IGSM/AgERA5 sample are used to drive the emulator and assess changes in average yields, yield variability, and the frequency of low-yield years across PNG. Our analysis shows that taro appears to be sensitive to both low- and high-rainfall levels during particular phases of growth and is sensitive to heat during particular phases, as well.

Our visit to farmers fields in the Markham Valley along with discussions with experts at GrowPNG in Lae, NARI, and PNG University of Technology in Lae alerted us to the fact that drought was a serious problem for taro, but the model revealed the additional issues with high rainfall and high temperature, along with the additional information about the months that were particularly important for determining the degree of damage that adverse weather might do to yields.

National-average yield changes by mid-century under high-emissions scenarios are projected to be small based on the median projections across climate models, however one of the climate models projects a much larger temperature increase relative to the other models, and for that climate model, the yield reduction is around 9% on average.

Keywords: Taro, yield emulator, crop modeling, climate change, Papua New Guinea, fixed-effect polynomial regression.

INTRODUCTION

Climate change poses a major threat to agricultural production globally, affecting crops through gradual stressors such as rising temperatures, shifting rainfall patterns, and sea level rise, as well as through more frequent and intense extreme weather events (Iese et al., 2020). These changes disrupt crop growth cycles, reduce yields, and threaten food security, particularly in regions where agriculture is central to livelihoods.

Papua New Guinea (PNG), an island nation in the western Pacific, is vulnerable to these challenges. Most of the population of PNG relies on subsistence agriculture for food security, with roots and tubers forming the staple of local diets (Benny et al., 2022). Among these crops, taro (*Colocasia esculenta*) is a staple crop, contributing an estimated 6% of total caloric intake for rural households based on HIES 2009/10 and Schmidt et al. (2024), with some FAO sources reporting higher figures (Rosegrant et al., 2024). Despite the importance of taro to national food security, there is limited understanding of how climate change will affect taro yields in PNG. We found only one study which investigated these impacts (Rosegrant et al., 2015), and that was done based on earlier climate models. Given the dependence of rural households on taro, improving the understanding of climate risks to this crop is critical for designing effective adaptation strategies and supporting food security planning.

Reliable predictions of crop yield are crucial for tackling food security challenges and informing climate adaptation policies. Process-based crop models such as the Decision Support System for Agrotechnology Transfer (DSSAT) provide a framework for simulating taro growth and yield under diverse environmental and management conditions (Jones et al., 2003; Hoogenboom et al., 2019; Hoogenboom et al., 2024). However, running DSSAT at high spatial resolution across many climate scenarios and planting

dates is computationally intensive, which limits its direct use in large-scale or long-term climate impact assessments (Franke et al., 2020).

To address this constraint, this paper develops a crop yield emulator for taro in Papua New Guinea. The emulator uses a fixed-effects polynomial regression trained on DSSAT simulations to approximate taro yields and provide a practical method for estimating future risks. This approach provides a computationally efficient tool for projecting taro yields under future climates and supports the assessment of climate risks to taro in PNG and can inform the design of targeted adaptation strategies.

The remainder of this paper is organized as follows: Section 1 reviews the existing literature. Section 2 details the materials and methods, including the DSSAT crop modeling framework, the specification of the taro yield emulator, and the integration of climate data. Section 3 presents the results, focusing on the sensitivity of taro to rainfall and temperature, as well as the implications of climate variability and climate uncertainty for yield variability and the frequency of low-yield events. Finally, Section 4 offers concludes.

CLIMATE CHANGE IMPACTS ON TARO: REVIEW OF APPROACHES AND FINDINGS

Taro (*Colocasia esculenta*) is a critical food security crop in Pacific Island households, yet climate change threatens production across the region. Although it is well-adapted to tropical temperatures (25–35°C), its high water requirement makes it vulnerable to both ends of the hydrological spectrum. In Papua New Guinea, excessive moisture promotes corm rot and taro leaf blight (Taylor et al., 2019), whereas water scarcity leads to the development of characteristic 'dumb-bell' shaped corms, signaling severe moisture stress (Onwueme, 1999).

In a study by Rosegrant et al. (2015), the Decision Support System for Agrotechnology Transfer (DSSAT) was used to project yield changes by the year 2050 under the IPCC AR4 A1B scenario. In three countries, taro was projected to suffer significant yield losses under climate change. In Fiji, worst-case losses are estimated between 12.3% and 17.5%. In PNG, losses are projected at 13%, and in the Solomon Islands, up to 16.1%. It was suggested in the paper that shifting to optimal cultivars and planting months can reduce these losses by approximately half (Rosegrant et al., 2015). Crimp (2017) developed the APSIM-Taro module, a process-based model with field data from Fiji, Vanuatu, and Tonga. Simulations revealed that taro maturity advances ~2 weeks per 1°C warming, causing 10–12% yield losses at +3°C. Elevated CO_2 partially mitigates these losses through improved water and radiation use efficiency, though it reduces nutritional quality (corm zinc, leaf protein) while enhancing palatability. Taro also demonstrates salt tolerance, with yield declines only above 150–200 mM NaCl.

Kodis et al. (2018) applied ecological niche models (ENMs) to identify climate-resilient taro cultivation areas in Hawaii. By integrating bioclimatic variables, topography, soil properties, and anthropogenic factors (urbanization, agricultural land use), their anthropogenic-inclusive model better predicted suitable cultivation zones under future climate scenarios. These findings demonstrate ENMs' utility for guiding biocultural conservation and site selection in Pacific Island contexts. However, integrated, region-wide dynamic models for atolls remain lacking, limiting adaptive capacity amid increasing climate variability

MATERIALS AND METHODS

DSSAT Crop Modeling System and Climate Models

This study uses the Decision Support System for Agrotechnology Transfer (DSSAT) crop modeling system to simulate taro yields under both historical and projected climate conditions. DSSAT is a widely-used, process-based crop simulation platform that models crop growth, development, and yield as functions of weather, soil, management, and cultivar characteristics (Jones et al. 2003; Hoogenboom et al. 2019; Hoogenboom et al. 2024).

For these simulations, we select a single representative taro variety to cover the entire study area. Other DSSAT taro varieties produce similar spatial yield patterns, but the variety labeled IB0002 BUN LONG was chosen because it consistently produces higher yields across most locations. DSSAT simulations are conducted for every pixel in PNG and nearby areas at a spatial resolution of 0.1°, resulting in 5,821 land pixels. To represent the diversity of planting practices in PNG, we simulate a sequence of planting dates at 10-day intervals throughout the calendar year, starting on 1 January. Taro is commonly planted in October and November in many parts of PNG. For the development of the emulator, we extract yield outputs from four representative planting dates: 10 days after December 31 (day 10, which is January 10), day 100, day 190, and day 280. These four planting windows sample a broad range of seasonal rainfall and temperature conditions and form the core training dataset for the emulator. Management practices in all simulations reflect low-input, rainfed conditions consistent with predominant smallholder production systems in PNG. Based on stakeholder interviews, taro producers apply little to no fertilizer on taro gardens, hence no nitrogen fertilizer is applied in the model. The model was initialized to represent a previously cultivated soil condition , characterized by a low initial nitrogen mass (20 kg N ha). This setting reflects the high nitrogen turnover and significant leaching typical of the region's humid tropical climate, alongside moderate levels of residual biomass (500 kg ha root mass and 250 kg ha surface residue).

Historical weather inputs are derived from the Multi-Source Weather (MSWX) gridded dataset (Beck et al., 2022) for calendar years 1980–2024. MSWX provides all necessary variables for running DSSAT, including solar radiation at the surface, precipitation, daily maximum temperature, and daily minimum temperature.

We initially used the HC27 global soils dataset (Koo and Dimes, 2010) as input for DSSAT. However, the simulations produced unrealistically large yield reductions under higher rainfall conditions, which when we consulted with NARI and university taro experts, it was judged to be inconsistent with taro performance. To address this, we replaced the HC27 soils with a single high-yielding soil profile from the WISE (World Inventory of Soil Emission Potentials) database, selected to better represent productive taro soils in PNG. The WISE database, developed by the International Soil Reference and Information Centre (ISRIC), provides a global repository of soil profiles (Batjes, 1995, 2002) that have been systematically formatted for use in ecophysiological models. This integration was facilitated by Gijsman et al. (2007), who converted 1,125 profiles from WISE Version 1.0 into the Decision Support System for Agrotechnology Transfer (DSSAT) format (Jones et al., 2003; Hoogenboom et al., 2014). This effort was later expanded by Romero et al. (2012), who converted and error-checked 4,382 profiles from WISE Version 1.1 for DSSAT compatibility. From this validated collection, we selected a high-yielding soil profile (labeled WS_000974 in our study; originally WI_ACPG024 in the WISE database) to serve

as a representative proxy for productive taro soils. This profile is based on field observations from a location in Papua New Guinea (6.033°S, 145.367°E) and is classified as a gleyic acrisol. This profile is then applied uniformly across the DSSAT simulations.

The DSSAT simulations described above generate grid-cell-level taro yields for each of the four selected planting dates and across both historical and scenario-based future climates. These simulations form the training dataset for the taro yield emulator.

Taro Yield Emulator Model Specification

To address the computational demands of running DSSAT simulations across large spatial and temporal scales, we develop a crop yield emulator using a fixed-effects polynomial regression model in R. The emulator was trained to reproduce DSSAT-simulated taro yields using climate data, providing a rapid and flexible tool for analyzing climate-yield relationships across Papua New Guinea. We estimate the model with the 'fixest' package in R, which efficiently handles high-dimensional fixed effects.

The model is specified as:

$$\ln(\mathrm{Y}_{it}) = \alpha_i + \sum_{m=0}^{9}\sum_{k=1}^{4}\beta_{m,k}^{(R)}\left(rain_{m,it}\right)^k + \sum_{m=1}^{8}\sum_{k=1}^{4}\beta_{m,k}^{(T)}\left(tx_{m,it}\right)^k + \epsilon_{it} \quad \ldots\ldots\ldots 1$$

where:

- $\ln(\mathrm{Y}_{it})$ is the log-transformed crop yield for pixel i and year t
- $\beta_{m,k}^{(R)}$ and $\beta_{m,k}^{(T)}$: coefficient of rainfall and temperature, respectively, in period / month *m* (relative to the planting period / month, which is month 1) and raised to a power, k
- $rain_{m,it}$: bimonthly rainfall index for pixel i and year t, constructed as the sum of rainfall in month $m-1$ and month m (rain_1, …, rain_8)
- $tx_{m,it}$: mean daily maximum temperature in month *m* (tx_1, …, tx_8)
- α_i: grid-cell fixed effects,
- ϵ_{it}: error term.

The fourth-degree polynomial terms allow the emulator to capture non-linear and threshold responses of taro yield to climate, reflecting the crop's sensitivity to both cumulative and distributional effects of rainfall and temperature. The log transformation of yield stabilizes variance and allows interpretation of coefficients as approximate percentage changes.

To account for taro's long growing season and phenological sensitivity, we constructed nine overlapping bimonthly rainfall sums and eight consecutive monthly maximum temperature variables, each aligned to the crop's phenological window starting at the planting date. We use rainfall as a proxy for soil moisture, each bimonthly rainfall variable $rain_{m,it}$ is defined as the sum of rainfall in month $m-1$ and month m, allowing us to capture the short-term carry-over of water availability that is relevant for taro growth and yield. This design allows the emulator to distinguish sensitivity to rainfall and temperature at different stages of the crop cycle.

By integrating process-based simulation with statistical emulation, this methodology enables an efficient and spatially detailed way to assess how climate change impacts taro production in PNG. This is helpful when evaluating the impact across different climates at all locations in PNG where taro is grown.

Once trained, the emulator can be rapidly applied to multiple climate scenarios, planting dates, and regions, enabling large-scale, climate change impact assessments that would be computationally intensive with DSSAT alone.

Using the Emulator to Assess Climate Impact on Taro

CMIP6 Climate Models

Climate data for the baseline period were derived from the MSWX dataset, and future climates are from the Inter-Sectoral Impact Model Intercomparison Project phase 3b (ISIMIP3b) using selected models from the Coupled Model Intercomparison Project Phase 6 (CMIP6). ISIMIP3b provides downscaled climate data from five global climate models (GFDL-ESM4, IPSL-CM6A-LR, MPI-ESM1-2-HR, MRI-ESM2-0, and UKESM1-0-LL). In this study, we restricted our analysis to the highest emissions scenario SSP585 (shared socioeconomic pathway). The climate data were then passed through the taro yield emulator at each pixel in Papua New Guinea to estimate projected changes in taro yields under SSP5-8.5, across the ensemble of ISIMIP3b models.

MIT-IGSM Climate Ensemble

To explore climate variability and extremes beyond a few discrete Global Climate Models (GCMs), we also combined the emulator with a large ensemble of future climates constructed from the MIT Integrated Global System Model (MIT-IGSM) and the AgERA5 historical dataset. AgERA5 provides gridded historical agro-meteorological data; we used 43 years (1979–2021) of monthly series to characterize observed variability. The MIT-IGSM provides an ensemble of 11,600 high-frequency distributions (HFDs), which can be viewed as representations of possible future climate states under a given emissions pathway.

We generated a large pool of candidate future climates by combining the MIT-IGSM HFDs with detrended monthly anomalies from AgERA5, yielding over 500,000 possible monthly climate trajectories. From this pool, we drew a random sample of 1,000 future climate realizations. For each of these 1,000 climates and for each pixel in PNG, we derived monthly rainfall and temperature values to compute taro yields. This approach allows us to quantify how changes in the distribution of climate variability and extremes may affect taro yield risk, including metrics such as low-yield percentiles, without the intensive computation of running DSSAT for every climate realization.

The high-emissions scenario used for the MIT-IGSM ensemble represents a strong warming pathway but is somewhat less extreme than SSP585 (i.e., RCP8.5), aligning approximately between RCP6.0 and RCP7.0 in terms of radiative forcing. Together, ISIMIP3b multi-model projections and the MIT-IGSM ensemble provide complementary insights into how the climate change trend and climate variability affect taro production in PNG when evaluated through the taro yield emulator.

RESULTS

This study provides a comprehensive assessment of how rainfall and temperature affect taro yields throughout the growing season in Papua New Guinea. Our findings are structured into several key sections: (1) analysis of rainfall and temperature impacts on taro yield, including threshold identification and marginal yield changes across growth stages (Figure 1); (2) spatial maps of projected percent taro yield change under five global climate models for the RCP8.5 scenario (Figure 2) and percent change

in taro yield from climate change by region, 2005-2050 (Table 1); (3) percent change in median taro yield per pixel under the high-emissions scenario of the MIT-IGSM from 2020 to 2050 (Figure 3); (4) percent change in taro yields from climate change at various points in the distribution, 2020-2050, under the high-emissions scenario (Table 2); and (5) frequency in 2050 of a 1-in-20 year low-yield event from 2020. The following sections discuss these findings in detail, supported by figures and tables that highlight key trends and insights.

Impact of rainfall and temperature

Figure 1 presents how rainfall and temperature affect taro yield throughout the growing season. The figure combines four plots to illustrate the effects of rainfall and temperature on taro yield across key growth stages. For the temperature graphs, month 1 is the mean daily maximum temperature (tx) for the month taro was planted, month 2 is tx for the month after that, etc. For rainfall graphs it is slightly more complicated. We believe that soil moisture rather than rainfall itself is the actual determinant of yield. As a proxy for soil moisture, we use the sum of rainfall in the current month and the preceding month. Therefore, period 1 sums the rainfall of the planting month (month 1), and the month prior to planting (month 0). Period 2 sums the rainfall from month 2 and month 1, and so on, through to period 8, after which we harvest the taro. We also believe that the moisture in the soil prior to planting is of critical importance, so period 0 rainfall is included in the regression and graph. The relationships shown in Figure 1 are derived from the fixed-effect polynomial regression results presented in Appendix Table A1, which quantify the stage-specific and nonlinear responses of taro yield to both rainfall and temperature throughout the crop cycle. The endpoints of each curve represent the 5th and 95th percentiles of observed climate data, so results outside these bounds should be interpreted with caution.

Figure 1 illustrates how taro yield responds to monthly rainfall and temperature relative to a 100% theoretical optimum. For example, in Period 3, the curve peaks at 400 mm of rainfall; a location receiving this amount achieves its maximum potential yield. If rainfall deviates to 300 mm or 600 mm, yield drops to 93% or 89%, respectively, showing that both moisture deficits and excesses can be detrimental. Calculating yield losses becomes more complex when a location’s normal climate is less than optimal. If a site normally receives 300 mm (93% yield) but drops to 200 mm (76% yield) in a dry year, the 17-percentage-point drop represents an 18% reduction relative to that site's normal output. Conversely, a shift from 450 mm to 350 mm might result in no loss at all because both points sit near the curve’s flat peak. What is important is the slope between the normal climate point for a location and the actual point in a given year.

To simplify these calculations, the "marginal change" curve plots the slope of the yield response curve directly. By using a trapezoidal approximation, averaging the marginal values at two points and multiplying by the climate distance between them, one can quickly estimate percentage changes. For instance, for period 3 rainfall, moving from 300 mm to 200 mm yields an average marginal value of 0.20, which, when multiplied by the 100 mm difference, suggests a 20% reduction. This closely aligns with the 18% we just derived from the yield response curve, confirming that while the response curve is better for identifying optimal conditions, the marginal curve is a more efficient tool for quantifying specific climate-driven yield shifts.

The top-left plot shows that taro yields are highest when bimonthly rainfall is around 400 mm for most 2-month periods in the growing season. The most pronounced yield decline for high rainfall occurs in period 3 when rainfall exceeds the 400mm threshold. It is also true that the most pronounced yield de-

cline for low rainfall occurs in period 3. We note that in the period immediately before planting, any increase in rainfall is associated with higher yields, highlighting taro's reliance on adequate soil moisture at establishment. Periods 2 and 8 show a preference for higher rainfall, while most other months show lower yields for rainfall levels above a threshold.

Figure 1: Crop yield response to rainfall and mean daily maximum temperature and percent change in crop yield for marginal change in temperature (°C) and rainfall (mm).

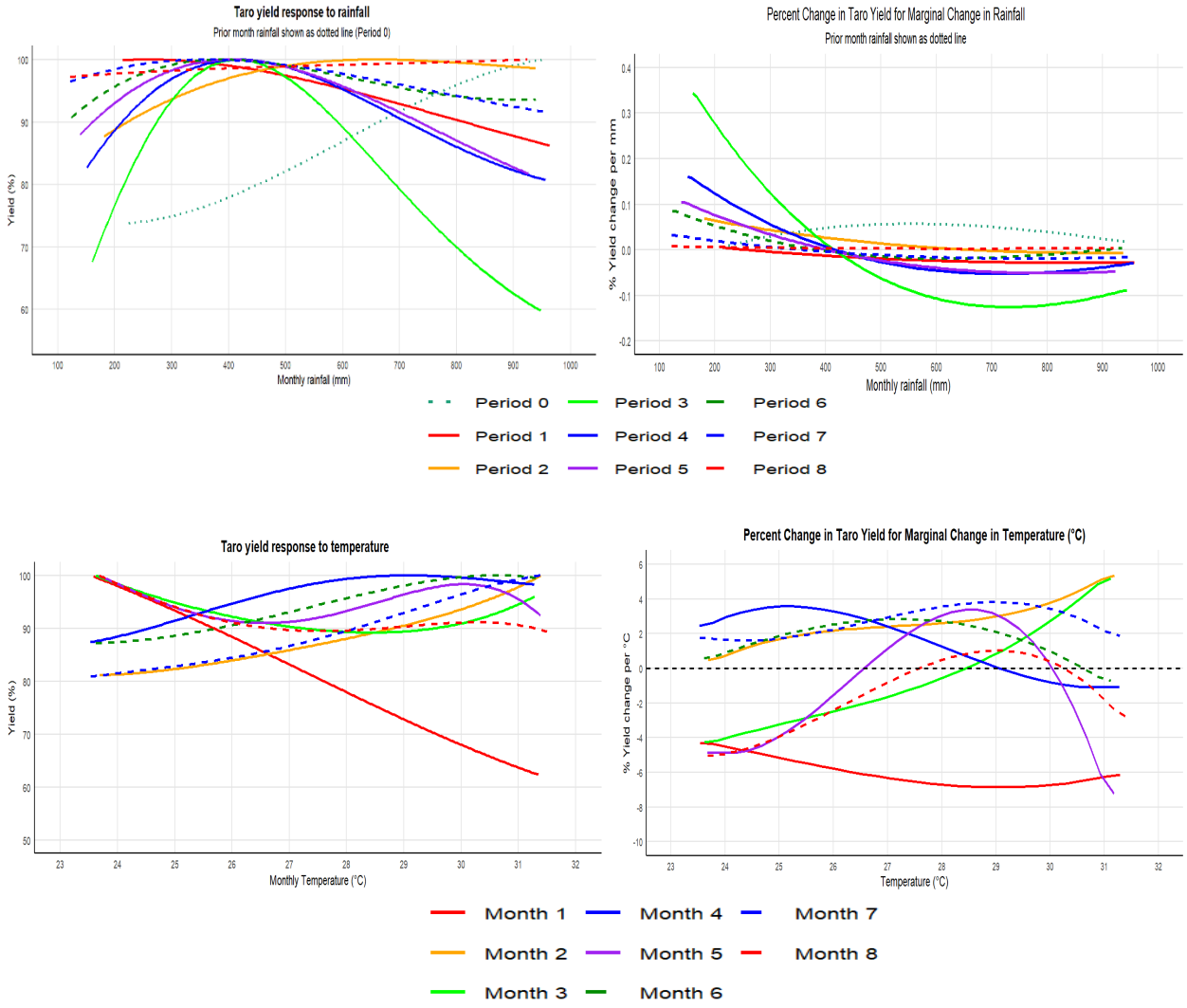

Notes: Yields are modeled across the 5th to 95th percentile range for both temperature (°C) and rainfall (mm) in each month.

The top-right plot shows the marginal effect of rainfall, representing how yield changes with an additional unit of rainfall. In other words, this plot demonstrates the slope of the curves in the top-left panel. Steeper slopes translate into larger marginal effects. Just as taro yields decline when rainfall is excessive, they also decline when it is insufficient, and the emulator suggests that the quantitative impact of drought is often larger than that of excess rainfall. For example, in period 3 (the bimonthly window covering months 2 and 3), the marginal effect peaks at about 0.34% yield increase per additional millimeter of rainfall around 160 mm. The marginal-effect curves clearly show that drought has particularly adverse effects in months 3 to 6, with month 3 being especially sensitive to low rainfall.

Figure 2: Change in precipitation (millimeters) in key climate models, circa 2005-2050, gridded

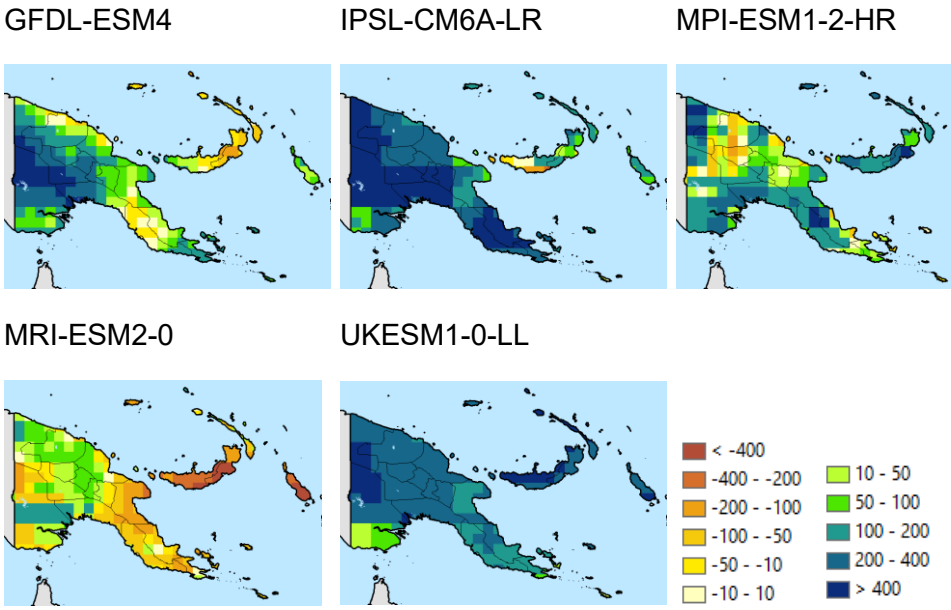

Source: NASA (2022) and ISIMIP (2021).

Figure 3: Change in temperature (^{0}C) in key climate models, circa 2005-2050, gridded

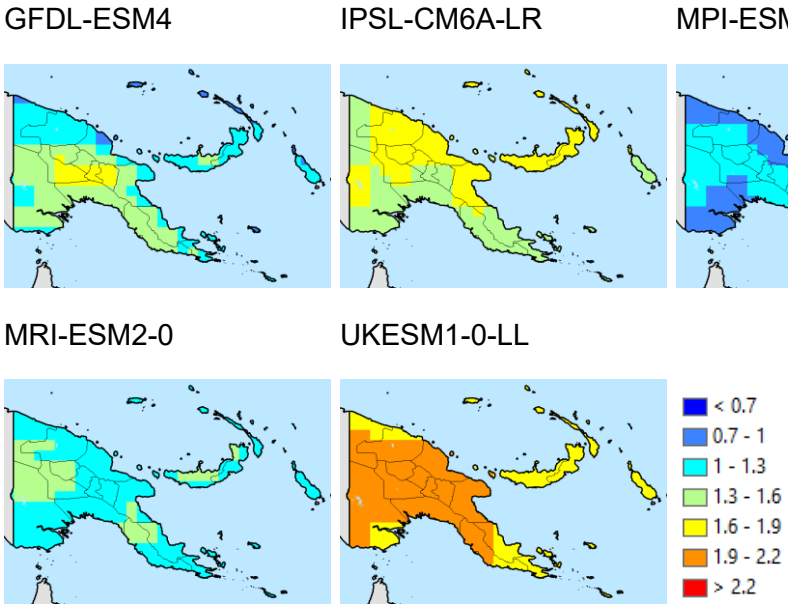

Source: NASA (2022) and ISIMIP (2021).

The bottom panels show that taro yield responses to the mean daily maximum temperature are strongly stage specific. In month 1 (the planting month), yields are highest at relatively cooler temperatures, around 23–24°C, with a steep decline as temperatures rise. Similar preferences for cooler conditions are observed in months 3, 5, and 8. In contrast, in months 2, 4, 6, and 7, yields increase with rising temperatures up to an optimum of roughly 29–31°C. The bottom-right panel, which plots the marginal effect of temperature, shows these patterns. For instance, in month 1, the curve remains entirely below zero across the observed temperature range, indicating that higher temperatures consistently reduce

yield during this initial stage. Specifically, if month 1 temperatures are around 28°C and increase by 1°C, the emulator projects an almost 7% reduction in yield.

Figures 2 and 3 shows the change in precipitation and temperature projected at each location in each of the climate models for the 2005-2050 period. Figure 2 shows that IPSL-CM6A-LR and UKESM1-0-LL project more rainfall than other models. Figure 3 shows temperature changes between 2005 and 2050. The UKESM1-0-LL projects more temperature change than any of the other models.

Figure 4 shows the projected percentage change in taro yield across PNG by 2050 under a high-emissions climate scenario (RCP8.5), as simulated by five global climate models and evaluated with the taro yield emulator. Yield changes are expressed as percent differences relative to a historical baseline period of 2005. The maps use a color-coded scale, with reddish brown indicating substantial yield declines (less than −10%) and blue indicating yield increases (greater than 10%), providing a spatially explicit view of future climate impacts on taro production. Yield changes are only reported for locations which currently grow taro.

Figure 4: Percent change in yield from climate change, 2005-2050, gridded

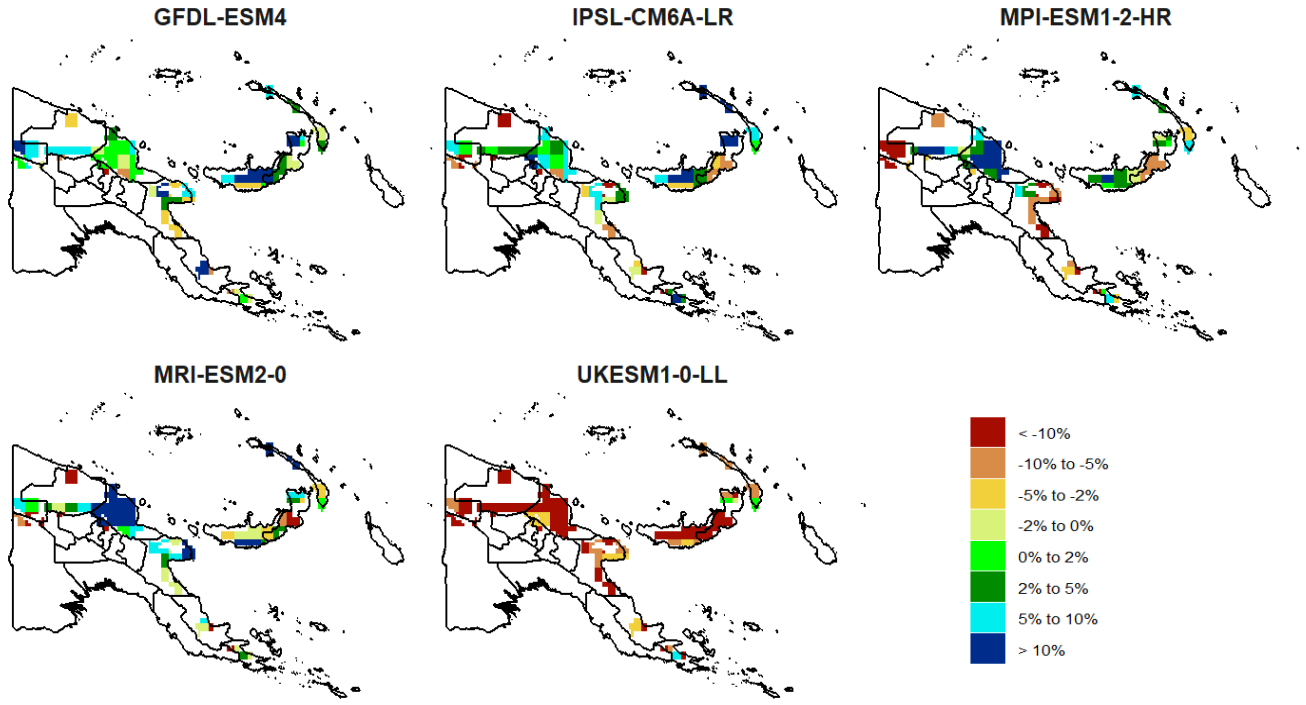

Source: Authors.

The results reveal considerable variation in projected yield changes across GCM models. The UKESM1-0-LL model projects the most pronounced yield declines, with extensive areas showing reductions greater than 10%. The MPI-ESM1-2-HR model also indicates widespread negative impacts, although fewer areas are affected and the magnitude of yield loss is generally less severe compared to the UKESM1-0-LL model. These outcomes are not as a result of the emulator framework, but rather a direct reflection of the differing climate forcing signals provided by each GCM.. When comparing maps showing projected temperature and precipitation changes for each GCM (see Figures 2 and 3), it appears clear that the losses in the UKESM1-0-LL model are driven almost exclusively by temperature rise, while the losses in the MPI model are driven almost exclusively by precipitation reduction.

In contrast, the GFDL-ESM4, IPSL-CM6A-LR, and MRI-ESM2-0 models show more mixed outcomes, with large regions exhibiting neutral or modestly positive yield changes, suggesting that some parts of PNG may experience limited losses or even slight gains under future climate conditions. These differences highlight the uncertainty inherent in climate projections and the importance of considering multiple models when assessing future risks.

Table 1 summarizes the projected percentage change in taro yields between 2005 and 2050 across Papua New Guinea, based on emulator outputs driven by five CMIP6 global climate models. For each region–model combination, the table reports the projected yield change for the IPSL-CM6A-LR model in a separate column, and the distribution of outcomes across all five models in terms of the minimum, median, and maximum values. This layout allows direct comparison between a single "best-matching" climate model and the broader ensemble, while explicitly representing uncertainty about future climate conditions.

We emphasize IPSL-CM6A-LR because comparisons with observed climate over 2000–2024 suggest that it reproduces recent trends in Papua New Guinea more closely than the other four models (Braide, Thomas, and Robertson 2026). The median across models is useful as a central estimate in the face of a small sample and large uncertainty, whereas the minimum-maximum range highlights how sensitive projected yields are to the choice of climate model. At the national level, the uncertainty ranges from a loss of 14% to a gain of 11%, revealing a 25-percentage point spread. This uncertainty demonstrates the risk of over-investing in solutions that only work in one possible future climate rather than investing in a suite of solutions that address various potential future realizations.

Table 1: Percent change in taro yield from climate change by region, 2005-2050

Region	IPSL	Median (%)	Minimum (%)	Maximum (%)
Nation	1.7%	2.3%	-13.9%	11.3%
Highlands	8.7%	4.2%	-7.8%	8.7%
Islands	3.1%	3.1%	-13%	3.7%
Momase	1.4%	2.1%	-14.4%	14.7%
Southern	-3.2%	-4.4%	-12.3%	-0.2%

Source: Authors.

The minimum (negative) yield changes at both the national and regional levels are consistently produced by the UKESM1-0-LL model. These negative outcomes show that under some possible climate futures climate change could substantially reduce taro yields. At the national level, both the IPSL-CM6A-LR model and the median across all five models indicate a small positive effect of climate change on average taro yields by 2050, on the order of 2%. Regional patterns reflect where taro is grown. According to IPSL-CM6A-LR, the Highlands region shows the largest relative gains, with yields increasing by almost 9%. While Highlands taro is sought after in highlands markets and Port Moresby, overall production area in the Highlands is currently limited. Southern also has relatively little taro area and is projected to experience yield decline of about 3%. Most taro production is concentrated in Momase and the Islands, where the IPSL-based projections suggest small average gains of around 1% and 3%, respectively. Taken together, these results indicate that, under central (median) climate projec-

tions, climate change is likely to have a limited positive effect on taro yields in PNG. However, it is important to note that substantial yield losses remain possible under some climate models and thus should be considered in adaptation planning.

Climate uncertainty and variability: impact on taro yield variability and low-yield events

Given the uncertainty across climate models and the non-linear relationship between climate and taro yields, we need to evaluate the combined effects of climate trends, model uncertainty, and future inter-annual variability on yield distributions. Figure 5 shows the median taro yield change between 2020 and 2050, derived from applying the emulator to 1,000 climate realizations from the MIT-IGSM and AgERA5 under a high-emissions scenario. Under this scenario, many pixels experience median yield losses (indicated by dark red and orange, ranging from < −7% to −1%), while others show clear median yield gains (green to blue bins, from 1% to ≥7%). A band of near-zero change (−1% to 1%, yellow) also persists, marking locations where the upward and downward effects of climate change are approximately offset. These results illustrate how adding a high-emissions trend to existing climate variability shifts the central tendency of yields and creates spatial contrast between areas likely to experience yield losses and those that may benefit.

Figure 5: Percent change in median taro yield per pixel under high emission from 2020 to 2050

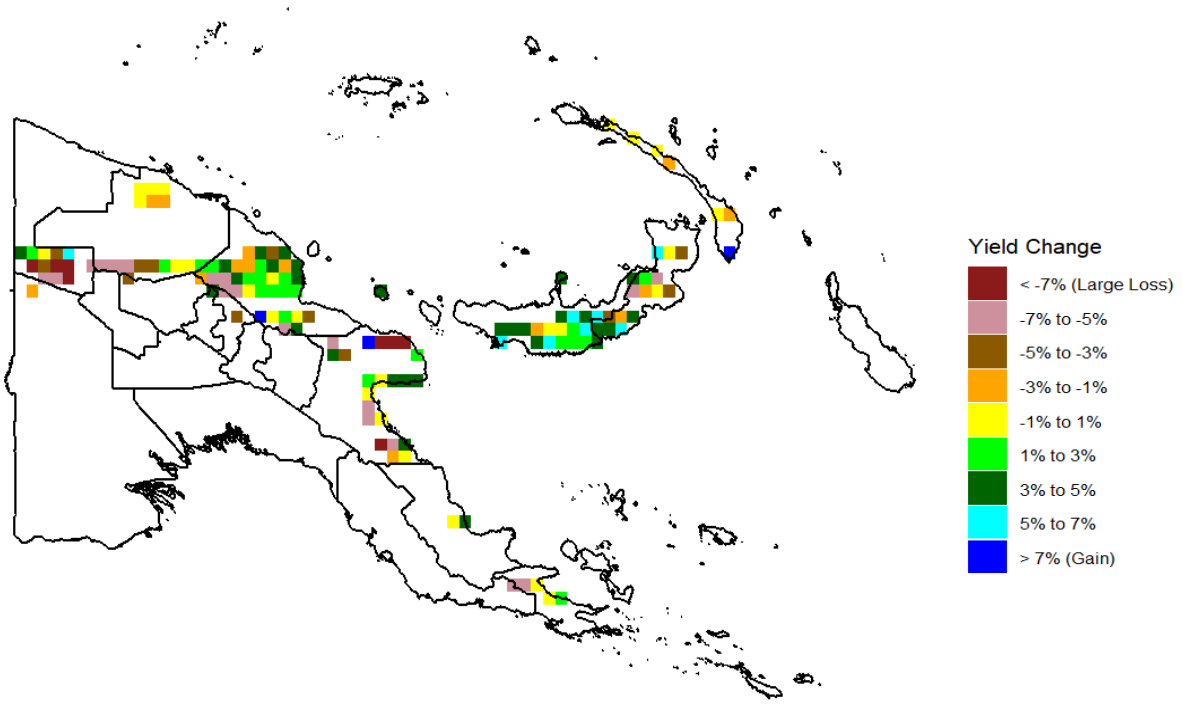

Table 2 summarizes how climate change affects taro yields across the yield distribution at national and regional scales between 2020 and 2050 under the high-emissions scenario, using the emulator projections from the MIT-IGSM climate ensemble. It also shows how much lower yields can be in a “bad” year (1-in-20 or 5th percentile) compared to a normal year (median). Nationally, climate change has only a small impact on normal yields, with the median and 5th percentile both declining by just 0.7%. The ratio of the 5th percentile to the median remains at about 90%, indicating that the severity of 1-in-20 “bad”

years relative to normal years changes very little for PNG. Regional patterns are more pronounced. In median years, yields increase by 2.7% in the Islands, but decline by 2.4%, 1.4%, and 4.0% in the Highlands, Momase, and Southern regions, respectively. The 5th percentile-to-median ratio in the Highlands drops from 78.4% to 76.1%, and in Southern it remains very low at about 72% in both years, indicating relatively high bad-year losses, even though taro area is limited in these regions. By contrast, the 5th-to-median ratios in the main taro-growing regions (Islands and Momase) remain stable (around 76–77% and 89–90%), suggesting that climate change has only a modest effect on the relative depth of bad years where most taro is currently grown. It also tells us that Momase appears to have much lower yield variability than the other regions.

Overall, these results show that under the high-emissions scenario, climate change is projected to have only modest effects on median taro yields in PNG, but regional differences in yield variability and the depth of bad years remain important, especially in the Highlands, Islands, and Southern regions.

Table 2: Percent change in taro yields from climate change at various points in the distribution, 2020-2050, under the high-emissions scenario

Unit of analysis	Year	Mean	5th percentile	25th percentile	Median	75th percentile	95th percentile	Percent of median in 5th percentile
National	2020	3416	3072	3234	3405	3557	3860	90.2%
National	2050	3409	3049	3232	3382	3569	3853	90.2%
Highlands	2020	3841	2949	3341	3760	4115	5367	78.4%
Highlands	2050	3770	2793	3280	3671	4096	5200	76.1%
Islands	2020	3415	2563	2977	3328	3810	4657	77.0%
Islands	2050	3477	2605	3066	3417	3845	4574	76.2%
Momase	2020	3426	3018	3283	3379	3556	3829	89.3%
Momase	2050	3393	3002	3236	3351	3540	3819	89.6%
Southern	2020	3074	2247	2841	3131	3262	3728	71.8%
Southern	2050	2971	2174	2748	3005	3163	3673	72.3%

Source: Authors.

Figure 6 shows how frequently the 5th-percentile (1-in-20-year) low-yield event, defined from the 2020 yield distribution, is expected to occur under 2050 climate conditions. Areas where climate change worsens the impact of bad weather, as indicated by an increase in the frequency of low-taro yield events, are given by orange, brown, and red colors, with red being the most severe (though compared to outcomes from other studies focusing on maize in Africa, these are relatively moderate). In contrast, large areas are projected to see less frequent low-taro yield events, with dark blue indicating that such events occur less often than once every 28 years. Overall, while some hotspots face an increased risk of low yields, a greater number of locations are projected to experience a reduction in the frequency of low-taro yield events under the 2050 climate.

Figure 6: Frequency in 2050 of a 1-in-20-year low-taro yield event from 2020.

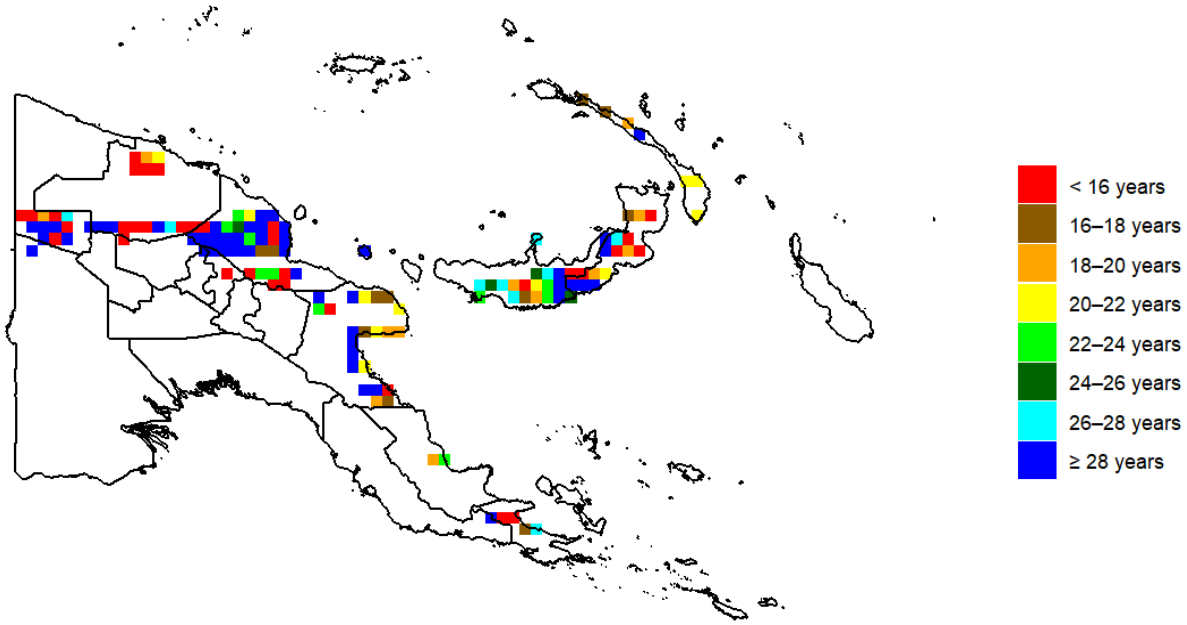

CONCLUSION

This paper developed and applied a taro yield emulator to assess the impacts of climate change on taro production in Papua New Guinea. By emulating DSSAT simulations with a fixed-effects polynomial regression, we created a computationally efficient tool that captures non-linear, stage-specific responses of taro yields to rainfall and temperature. Using ISIMIP3b climate models and a large MIT-IGSM ensemble, the emulator enabled us to evaluate both average yield changes and the distribution of low-yield outcomes across pixels and time.

The results show that taro in PNG is sensitive to both rainfall and heat stress, but that national-average impacts on yields to 2050 are modest under high-emissions scenarios. Across the five ISIMIP3b models, the largest yield losses at both national and regional scales are consistently produced by UKESM1-0-LL. In contrast, the median and IPSL-CM6A-LR show small national gains of around 2% over 45 years, with slight positive or near-neutral effects in major taro production regions of Momase and the Islands. However, the range across models is wide (approximately −14% to +11% nationally), highlighting substantial climate model uncertainty. The MIT-IGSM sample similarly finds small changes in national median yields and in the severity of 1-in-20 low-taro yield years, but reveals important regional contrasts, including more frequent bad years in the Highlands and persistently high downside risk in the Islands and the Southern region.

Overall, these findings suggest that climate change to 2050 is unlikely to cause large average declines in national taro yields, but that localized hotspots of vulnerability and large model uncertainty remain. Taro food security in PNG appears relatively robust in aggregate, yet exposed to significant regional risk under some plausible futures.

Investments in drought-, flood-, and heat-tolerant varieties can be helpful not simply in adapting to climate change but also to reduce yield variability due to climate variability. Finally, the emulator framework should be extended to additional varieties, management options, and lower-emissions scenarios,

and complemented with improved observational data, to better support climate-informed planning for taro and other staple crops in Papua New Guinea.

ABOUT THE AUTHORS

Tamunotonye M. Braide is a senior research officer in the Foresight and Policy Modeling unit of IFPRI and is based in Pretoria, South Africa. Timothy S. Thomas is a senior research fellow in the Foresight and Policy Modeling unit of IFPRI and is based in Washington, DC, USA. Richard D. Roberston is a research fellow in the Foresight and Policy Modeling unit of IFPRI and is based in Illinois, USA.

ACKNOWLEDGEMENTS

The authors would like to acknowledge the support of by the Australia Department of Foreign Affairs and Trade (DFAT) through the Australia High Commission (AHC) in Port Moresby, and the Australian Center for International Agricultural Research (ACIAR). They would also like to thank Harry Gimiseve, Dave Stewart, Julie Sip, Ruthy Kusak, with farmer field visits and vital information on taro production; and Tom Okpul, Birte Nass-Komonong, Laurie Fooks, and Peter Gendua expert advisement on the current state of taro in PNG.

REFERENCE

Batjes, N.H., 1995. A homogenized soil data file for global environmental research: A subset of FAO, ISRIC and NRCS profiles (Version 1.0) (No. 95/10b). ISRIC.

Batjes, N.H., 2002. A homogenized soil profile data set for global and regional environmental research. WISE, version 1.1.

Beck, H. E., A. I. J. M. van Dijk, P. R. Larraondo, T. R. McVicar, M. Pan, E. Dutra, and D. G. Miralles, 2022: MSWX: Global 3-Hourly 0.1° Bias-Corrected Meteorological Data Including Near-Real-Time Updates and Forecast Ensembles. Bull. Amer. Meteor. Soc., 103, E710–E732, https://doi.org/10.1175/BAMS-D-21-0145.1.

Benny, Dickson, Todd Benson, Mark Ivekolia, Mekamu Kedir Jemal, and Raywin Ovah. 2022. Improving agricultural productivity in Papua New Guinea: Strategic and policy considerations. Vol. 1. Intl Food Policy Res Inst.

Braide, Tamunotonye, Timothy S. Thomas, and Richard D. Robertson. 2026. “Climate Change and the Impact on Taro (Updated and Expanded)”, PNG Project Note, January 2026.

Crimp, S., 2017. Understanding the response of taro and cassava to climate change. Australian Government, Australian Center for International Agricultural Research.

Franke, J.A., Müller, C., Elliott, J., Ruane, A.C., Jägermeyr, J., Snyder, A., Dury, M., Falloon, P.D., Folberth, C., François, L. and Hank, T., 2020. The GGCMI Phase 2 emulators: global gridded crop model responses to changes in CO_2, temperature, water, and nitrogen (version 1.0). Geoscientific Model Development, 13(9), pp.3995-4018.

Gijsman, A.J., Thornton, P.K. and Hoogenboom, G., 2007. Using the WISE database to parameterize soil inputs for crop simulation models. Computers and Electronics in Agriculture, 56(2), pp.85-100.

Hoogenboom, G., Jones, J.W., Wilkens, P.W., Porter, C.H., Boote, K., Hunt, L., Singh, U., Lizaso, J.I., White, J.W., Ogoshi, R.M. and Koo, J., 2014, November. The Decision Support System for Agrotechnology Transfer (DSSAT) Version 4.6. In ASA, CSSA and SSSA International Annual Meetings (2014). ASA-CSSA-SSSA.

Hoogenboom, G., C.H. Porter, K.J. Boote, V. Shelia, P.W. Wilkens, U. Singh, J.W. White, S. Asseng, et al. 2019. “The DSSAT Crop Modeling Ecosystem.” In Advances in Crop Modeling for a Sustainable Agriculture, ed. K.J. Boote, 173–216. Cambridge, UK: Burleigh Dodds Science Publishing. https://dx.doi.org/10.19103/AS.2019.0061.10

Hoogenboom, G., C.H. Porter, V. Shelia, K.J. Boote, U. Singh, W. Pavan, F.A.A. Oliveira, L.P. Moreno-Cadena, T.B. Ferreira, J.W. White, J.I. Lizaso, D.N.L. Pequeno, B.A. Kimball, P.D. Alderman, K.R. Thorp, S.V. Cuadra, M.S. Vianna, F.J. Villalobos, W.D. Batchelor, S. Asseng, M.R. Jones , A. Hopf, H.B. Dias , A. Jintrawet, R. Jaikla , E. Memic , L.A. Hunt, and J.W. Jones . 2024. Decision Support System for Agrotechnology Transfer (DSSAT) Version 4.8.5 (www.DSSAT.net) . DSSAT Foundation , Gainesville , Florida, USA.

Iese, V. et al. 2020. Agriculture Under a Changing Climate. In: Kumar, L. (eds) Climate Change and Impacts in the Pacific. Springer Climate. Springer, Cham. ISIMIP. 2021. Downscaled GCMs. Downloaded August 16, 2021ISIMIP. 2021. Downscaled GCMs. Downloaded August 16, 2021.

Jones , J.W. , G. Hoogenboom , C.H. Porter , K.J. Boote , W.D. Batchelor, L.A. Hunt , P.W. Wilkens , U. Singh , A.J. Gijsman , and J.T. Ritchie . 2003. “ The DSSAT Cropping System Model . ” European Journal of Agronomy 18 (3–4) : 235–265 . https://doi.org/10.1016/S1161-0301 (02) 00107-7 .

Kodis, M.O., Galante, P., Sterling, E.J. and Blair, M.E., 2018. Ecological niche modeling for a cultivated plant species: a case study on taro (Colocasia esculenta) in Hawaii. Ecological Applications, 28(4), pp.967-977.

Koo, J., and Dimes, J. (2010). HC27 Soil Profile Database. Washington, DC: International Food PoliResearch Institute. Available online at: http://hdl.handle.net/1902.1/20299

MSWX. 2025. https://www.gloh2o.org/mswx/. Downloaded January 29, 2025.

NASA. 2022. "Global Daily Downscaled Projections (NEX-GDDP-CMIP6)". Downloaded June 1, 2022.

Romero, C.C., Hoogenboom, G., Baigorria, G.A., Koo, J., Gijsman, A.J. and Wood, S., 2012. Reanalysis of a global soil database for crop and environmental modeling. Environmental Modelling & Software, 35, pp.163-170.

Rosegrant, M.W., Valmonte-Santos, R., Thomas, T.S., You, L. and Chiang, C., 2015. Climate change, food security, and socioeconomic livelihood in Pacific Islands.

Rosegrant, Mark W., Timothy B. Sulser, Shahnila Dunston, Abhijeet Mishra, Nicola Cenacchi, Yohannes Gebretsadik, Richard Robertson, Timothy Thomas, Keith Wiebe. 2024. "Food and nutrition security under changing climate and socioeconomic conditions", Global Food Security 41. https://doi.org/10.1016/j.gfs.2024.100755.

Schmidt, Emily; Fang, Peixun; Jemal, Mekamu; Mahrt, Kristi; Mukerjee, Rishabh; Rosenbach, Gracie and Yadav, Shweta. 2024. 2023 PNG Rural Household Survey Report. Washington, DC: International Food Policy Research Institute. https://hdl.handle.net/10568/140437. https://doi.org/10.1007/978-3-030-32878-8_9

Taylor, M., Lebot, V., McGregor, A. and Redden, R.J., 2019. Sustainable production of roots and tuber crops for food security under climate change. Food security and climate change, pp.359-376.

APPENDIX A. FIXED EFFECTS POLYNOMIAL REGRESSION RESULTS

Table A1. Fixed-Effects Polynomial Regression Results for Taro

Variable	Estimate	Std.error	T-statistic	Significance
rain0	75.43869	1.75074	43.0896	***
rain0^2	-21.9962	1.464498	-15.0196	***
rain0^3	-10.1891	2.239964	-4.54878	***
rain0^4	32.47562	2.6184	12.40285	***
rain1	-42.8108	1.580329	-27.0898	***
rain1^2	-7.14609	1.319405	-5.41615	***
rain1^3	10.34921	1.476793	7.007896	***
rain1^4	-7.70291	1.633449	-4.71573	***
rain2	31.81246	2.083288	15.27031	***
rain2^2	-11.8053	1.857426	-6.35576	***
rain2^3	28.14102	2.414002	11.65742	***
rain2^4	-10.373	2.844945	-3.64613	***
rain3	-52.2639	2.071156	-25.2341	***
rain3^2	-88.1658	2.671549	-33.0018	***
rain3^3	107.2178	4.871674	22.00841	***
rain3^4	-105.73	5.667436	-18.6557	***
rain4	-10.2889	2.463836	-4.17597	***
rain4^2	-28.8662	2.605473	-11.0791	***
rain4^3	49.87409	4.046355	12.32568	***

rain4^4	-58.9612	11.43881	-5.15449	***
rain5	-25.8747	2.376991	-10.8855	***
rain5^2	-23.2925	1.722186	-13.525	***
rain5^3	47.33474	1.969091	24.03888	***
rain5^4	-33.0669	3.344712	-9.88632	***
rain6	5.180803	2.477413	2.091215	*
rain6^2	-13.5633	2.210707	-6.13527	***
rain6^3	12.6418	2.577291	4.905075	***
rain6^4	-36.6641	2.895552	-12.6622	***
rain7	-16.4357	1.96946	-8.3453	***
rain7^2	-8.74599	1.7867	-4.89505	***
rain7^3	13.0708	2.304459	5.671961	***
rain7^4	-13.6339	3.238618	-4.20979	***
rain8	7.773705	1.434715	5.418292	***
rain8^2	-1.1334	0.93306	-1.21471	
rain8^3	-0.19026	0.713478	-0.26666	
rain8^4	-2.32641	0.616002	-3.77663	***
tx1	-128.634	3.007298	-42.7739	***
tx1^2	-10.7259	1.703694	-6.2957	***
tx1^3	5.324025	1.171742	4.543684	***
tx1^4	2.154984	1.230934	1.75069	.
tx2	53.11839	3.425106	15.50854	***
tx2^2	20.36502	1.992972	10.21842	***
tx2^3	-0.61317	1.259107	-0.48699	
tx2^4	7.168828	1.24016	5.780565	***
tx3	-13.5116	2.98981	-4.51922	***
tx3^2	39.1922	1.87708	20.87935	***
tx3^3	7.362853	1.133598	6.495119	***
tx3^4	3.789608	1.05983	3.575675	***
tx4	28.33485	2.408598	11.76404	***
tx4^2	-14.6815	1.666488	-8.80987	***
tx4^3	-12.3426	1.12481	-10.9731	***
tx4^4	9.115657	0.979586	9.305622	***
tx5	-7.34205	2.975388	-2.46759	*
tx5^2	4.741756	2.16022	2.195034	*

tx5^3	-24.0577	1.483518	-16.2167	***
tx5^4	-33.2939	1.470846	-22.6359	***
tx6	35.90594	3.092088	11.6122	***
tx6^2	-2.19082	2.058367	-1.06435	
tx6^3	-14.4473	1.464039	-9.86811	***
tx6^4	-1.67911	1.442177	-1.16429	
tx7	61.00893	2.902971	21.01603	***
tx7^2	3.673048	1.391816	2.639033	**
tx7^3	-2.53571	1.003733	-2.52628	*
tx7^4	-9.58696	1.051336	-9.11883	***
tx8	-26.2981	2.906089	-9.04931	***
tx8^2	17.62068	1.83352	9.610301	***
tx8^3	-13.9309	1.465382	-9.50664	***
tx8^4	-15.2672	1.462306	-10.4405	***
RMSE	0.38896			
Adj R^2	0.470295			
Within R^2	0.382174			
Obs.	846659			

*** p < 0.001, ** p < 0.01, * p < 0.05, . p < 0.1

Note: rain0 is the sum of the 2 months prior to planting, capturing the importance of pre-planting soil moisture.

The Papua New Guinea (PNG) Agriculture, Food and Nutrition Policy Support Program (PNG-AFNP) is managed by the International Food Policy Research Institute (IFPRI) and is financially supported by the Australia Department of Foreign Affairs and Trade (DFAT) through the Australia High Commission (AHC) in Port Moresby, and the Australian Center for International Agricultural Research (ACIAR). This publication has been prepared as an output of PNG-AFNP and has not been independently peer reviewed. Any opinions expressed here belong to the author(s) and are not necessarily representative of or endorsed by IFPRI or the funding providers.

INTERNATIONAL FOOD POLICY RESEARCH INSTITUTE

A world free of hunger and malnutrition

IFPRI is a CGIAR Research Center

1201 Eye Street, NW, Washington, DC 20005 USA | T. +1-202-862-5600 | F. +1-202-862-5606 | Email: ifpri@cgiar.org | www.ifpri.org | www.ifpri.info